Mechanical Systems and Signal Processing 232 (2025) 112697

Contents lists available at ScienceDirect

Mechanical Systems and Signal Processing

journal homepage: www.elsevier.com/locate/ymssp

Modelling and stochastic updating of nonlinear structural joints

Pushpa Pandey [a],*, Nidhal Jamia [a], Tanmoy Chatterjee [b], Hamed Haddad Khodaparast [a], Michael Ian Friswell [a]

[a] Faculty of Science and Engineering, Swansea University, Wales, United Kingdom
[b] School of Mechanical Engineering Sciences, University of Surrey, England, United Kingdom

ARTICLE INFO

Communicated by H. Ouyang

Dataset link: https://github.com/maltekrack/NLtest

Keywords:
Likelihood function
Backbone curves
Stochastic nonlinear dynamics
Bayesian inference
Markov Chain Monte Carlo
Phase-locked loop
Deep learning

ABSTRACT

This paper presents a novel framework for modelling and stochastic updating of nonlinear systems in structural dynamics, with particular emphasis on joint structures. The key innovation lies in the integration of experimental data, system identification, and probabilistic methods to develop a comprehensive understanding of nonlinear dynamic behaviour. The methodology employs a specialised control system to extract backbone curves, which characterise the system's fundamental nonlinear response. A data-driven approach is implemented to identify the dominant system dynamics, which is then seamlessly integrated with the control system to create an analytical model. A significant contribution of this work is the development of a stochastic framework that combines the analytical model with measured system responses through probabilistic sampling methods, enabling robust uncertainty quantification. To address the computational challenges inherent in such complex simulations, the framework incorporates a deep learning model trained on both experimental and analytical data. This integration substantially improves computational efficiency while maintaining accuracy in predicting nonlinear dynamic responses. The framework's effectiveness is demonstrated through application to jointed structures, where traditional deterministic approaches often fall short. By providing a probabilistic perspective on system behaviour, this methodology offers more reliable predictions of dynamic responses under varying conditions. The successful implementation of this approach represents a significant advancement in the field of structural dynamics, particularly for complex systems where uncertainty quantification is crucial for accurate response prediction.

1. Introduction

Stochastic modelling is crucial in analysing non-linear systems in structural dynamics, especially jointed structures. These structures, prevalent in bridges, aircraft, and machinery, exhibit complex behaviours due to joints introducing non-linearities and uncertainties [1]. Traditional deterministic models often fail to predict performance and reliability accurately under real-world conditions, making stochastic methods essential [2]. The significance of stochastic modelling lies in its ability to account for inherent uncertainties in jointed structures. These uncertainties stem from material properties, geometric dimensions, boundary conditions, and external loads. Probabilistic methods in stochastic models provide a realistic representation of structural behaviour, enabling engineers to predict various responses under different conditions. This approach is vital for assessing the reliability and safety of structures subjected to dynamic loads.

Stochastic modelling and updating of linear and nonlinear systems have been extensively studied in recent decades. For linear systems, methods such as as Perturbation method [3], Kalman filtering [4,5] and Bayesian inference [6–8] have been widely applied.

* Corresponding author.
E-mail address: pushpa.pandey@swansea.ac.uk (P. Pandey).

https://doi.org/10.1016/j.ymssp.2025.112697
Received 25 October 2024; Received in revised form 11 February 2025; Accepted 2 April 2025
Available online 21 April 2025

In the realm of nonlinear systems, techniques like the extended Kalman filter [9–11], particle filters [12,13], and Markov Chain Monte Carlo (MCMC) methods [14–16] have shown promising results. Researchers have also explored the use of polynomial chaos expansion [17,18] and Gaussian process regression [8,19] for uncertainty quantification in nonlinear systems. In the context of jointed structures, studies by Jalali et al. [20] and Govers et al. [21] have demonstrated the effectiveness of stochastic model updating techniques in capturing the uncertainties associated with joint parameters and system responses.

Jointed structures are particularly prone to non-linear dynamic behaviour due to interactions at the joint interfaces, such as friction and contact stiffness [22]. Stochastic modelling addresses these challenges by considering variability in joint properties, leading to more robust analyses. Techniques like stochastic finite element methods (SFEM) [23] and Monte Carlo simulations [24] quantify the probability distributions of structural responses, aiding in better decision-making for design and maintenance.

A key concept in the analysis of non-linear jointed structures is the backbone curve, which represents the locus of periodic responses of the system under harmonic excitation. The backbone curve provides valuable insights into the system's non-linear behaviour, including bifurcations, stability boundaries, and potential for chaotic motions. However, accurately determining the backbone curve for jointed structures with complex non-linearities and uncertainties can be challenging using traditional analytical or numerical methods [25]. To address this challenge, researchers have explored the use of Phase Locked Loops (PLLs) for backbone curve extraction [26,27]. Making use of single-nonlinear-mode theory which focuses on the behaviour of a system when it predominantly exhibits a single mode of vibration, even in the presence of nonlinearities [26]. PLLs are adaptive control systems that can track and isolate the fundamental component of a periodic signal, even in the presence of non-linearities and distortions. By coupling PLL with appropriate excitation, it is possible to experimentally construct the backbone curve of a jointed structure, capturing its non-linear dynamics without relying on detailed mathematical models or simulations. This approach has shown promising results in applications such as structural health monitoring, vibration control, and design optimisation of jointed structures.

While PLL-based backbone curve extraction provides a powerful tool for characterising the non-linear behaviour of jointed structures, it is often desirable to obtain a mathematical model of the underlying system dynamics. This is where the Sparse Identification of Nonlinear Dynamics (SINDy) technique becomes relevant and useful. SINDy is a data-driven approach that leverages the sparsity of governing equations to identify the dominant terms and parameters of a non-linear dynamical system directly from measurement data [28]. SINDy's key advantage is identifying parsimonious models from high-dimensional data without prior assumptions about the governing equations. It formulates system identification as a sparse regression problem, using a library of candidate non-linear functions to represent system dynamics. Sparsity-promoting techniques select the most relevant terms, discarding insignificant ones, resulting in a sparse, interpretable model [29]. This data-driven approach enables SINDy to handle complex non-linear systems, including chaotic or multi-scale behaviours, making it valuable for analysing jointed structures with intricate non-linearities.

Extending SINDy's capabilities, the integration of analytical models with deep learning (DL) techniques provides a promising avenue for optimising computationally intensive simulations, such as Markov chain Monte Carlo (MCMC) methods. MCMC simulations are widely employed for uncertainty quantification and sampling from high-dimensional probability distributions but can be computationally demanding, especially for non-linear systems like jointed structures. This computational burden motivates the integration of analytical models derived from SINDy with DL architectures to accelerate MCMC simulations while maintaining physical consistency. By leveraging the interpretable models obtained from SINDy and incorporating them as physics-informed priors or constraints within DL frameworks, it becomes possible to accelerate MCMC simulations. This hybrid approach combines the strengths of data-driven and physics-based modelling, enabling efficient exploration of high-dimensional parameter spaces and accurate characterisation of uncertainties in jointed structures' behaviours.

This study builds upon a previously proposed framework published by the authors [30], in which the approximated likelihood in the Bayesian framework was initially introduced and validated using experimental data for which a physical model was available, where a physical model was available. It is well known that joints in structures are the primary source of both nonlinearity and variability in the dynamic responses of the structure. The challenge addressed in this paper lies in identifying a stochastic nonlinear model of the joints capable of predicting these behaviours from the responses of the structures. To this end, the proposed framework is extended to accommodate a different experimental system where a pre-existing computational model does not exist. It is demonstrated that integrating a deep learning component into the proposed framework marks a significant improvement in the methodology.

In this paper, a novel framework is proposed that integrates experimental backbone curve extraction using PLL, data-driven system identification with SINDy, and deep learning techniques to accelerate stochastic model updating of nonlinear jointed structures. The key contributions of this work encompass a methodology for extracting backbone curves of jointed structures using PLL, the application of SINDy for identifying parsimonious models of nonlinear jointed systems, the development of a hybrid analytical-DL approach for accelerating MCMC simulations in stochastic model updating. This integrated approach aims to advance the state-of-the-art in stochastic modelling of nonlinear jointed structures by providing more accurate and computationally efficient tools for structural dynamics analysis.

The proposed framework facilitates the prediction of the nonlinear and uncertain dynamic response of structural joints through the time response data and backbone curve. Time response data from the structure with joints is first used to identify the underlying deterministic nonlinear system using SINDy, which captures the essential nonlinear behaviours and joint characteristics in a reduced-order model. This identified model is then incorporated into a Bayesian framework alongside multiple experimental backbone curves, enabling the estimation of probability distributions for the identified reduced order model system parameters. By leveraging Bayesian inference, the inherent variability in jointed structures is systematically characterised. Once the parameter distributions are obtained

through MCMC sampling, probabilistic predictions of the nonlinear response, i.e. the probabilistic distributions of backbone curves, are determined.

The structure of this paper is as follows: Section 2 outlines the general framework, combining experimental data, analytical modelling, and DL methods. Section 3 details the experimental setup and the procedure for extracting backbone curves with PLL. Section 4 explains the system identification using SINDy, including the methodology and validation of the derived 1 Degree of Freedom (1-DOF) model. Section 5 covers the integration of the SINDy-derived 1-DOF model with PLL in Simulink to generate analytical backbone curves. Section 6 describes the DL model for computational optimisation, detailing its architecture, training, and performance. Section 7 discusses the stochastic model updating using DL model within a MCMC framework. Section 8 gives a thorough discussion of the results, comparing the efficacy of DL models in stochastic modelling. Lastly concluding the paper by summarising key findings, addressing limitations, and proposing future research directions.

2. Integrated analytical and DL framework for stochastic modelling

Before introducing the framework, it is crucial to understand the motivation behind its development. Stochastic model updating of nonlinear systems, particularly jointed structures, presents significant challenges due to the computational intensity of traditional methods. These challenges stem from the need to repeatedly evaluate complex nonlinear models within stochastic algorithms, often leading to prohibitively long computation times. The primary objective in developing this framework is to address these computational challenges while maintaining the physical interpretability of the model. A more efficient and accurate approach to stochastic modelling of nonlinear dynamic systems is aimed to be created by integrating analytical modelling with data-driven techniques.

In this study, a single degree of freedom (1-DOF) model is utilised for system identification and modelling. This simplification to a 1-DOF is chosen due to its computational efficiency and the ability to capture essential dynamics of the system for initial studies. The essential nonlinear dynamics can be captured by a 1-DOF model for many jointed structures, while computational complexity is significantly reduced. However, it should be noted that the framework can be extended to multi-degree of freedom (MDOF) systems. Such an extension would involve the identification of multiple modes and their interactions.

A key aspect of this framework is the use of DL to accelerate the stochastic model updating process. Stochastic model updating, particularly when MCMC methods are used, can be computationally intensive due to the need for numerous model evaluations. A surrogate model capable of rapid predictions is created by training a DL model on backbone curves generated from both experimental data and the analytical model. This DL surrogate can then be used within the MCMC algorithm, whereby computation time is significantly reduced.

It is important to emphasise that while this framework incorporates deep learning to enhance computational efficiency, the core process of stochastic model updating can be performed without the DL component. In such a case, the analytical model derived from SINDy would be directly used within the MCMC algorithm for stochastic model updating. This traditional approach, though more computationally intensive, maintains a direct link to the physics-based model throughout the entire process. The inclusion of the DL model in the framework serves as an optional acceleration technique, particularly beneficial for complex systems or when rapid analysis is required. By presenting both pathways – with and without DL – the framework offers flexibility in balancing computational speed with direct physical interpretability, depending on the specific requirements of the analysis.

With this context in mind, the framework shown in Fig. 1 that integrates both analytical and DL models for stochastic modelling of mechanical systems is now introduced. Time series data from experiments is utilised for system identification giving a 1-DOF model which is used by the PLL controller within Simulink to produce analytical backbone curves. These curves, along with experimental backbone curves, form a DL database used to train a DL model. The trained DL model predicts backbone curves, which are then validated against measured backbone curves. Finally, the framework employs stochastic modelling using MCMC techniques for model updating. This process leverages the predictive capabilities of the DL model for stochastic model updating of the system using its backbone curve as measurement data. By combining physical modelling with data-driven techniques and stochastic model updating, the framework provides a comprehensive solution for complex dynamic systems analysis.

The framework presented in Fig. 1 outlines a comprehensive approach to stochastic modelling of mechanical systems, integrating both analytical and DL methods. Below is a detailed explanation of the workflow:

1. **Data Collection and Preprocessing:** The experimental data is collected and stored in two databases i.e., the experimental database containing raw experimental data and the SINDy database that stores experimental time series data.
2. **System Identification:** The SINDy algorithm is applied to the time series data. This process yields a 1-DOF model of the system capturing the non-linearity.
3. **Analytical Model:** The 1-DOF model is implemented in Simulink. A PLL controller is integrated with the 1-DOF model. This setup generates analytical backbone curves, representing the system's nonlinear behaviour.
4. **DL Model Development:** A DL database is created, combining backbone curves processed from the experimental database and analytical backbone curves from the Simulink model. This database is used to train a DL model. The trained DL model can then generate backbone curves based on input parameters.
5. **Model Selection:** The framework allows the selection of either the analytical model or the DL model for further analysis.
6. **Stochastic modelling:** MCMC techniques are employed for stochastic modelling. This process uses Bayesian analysis to perform model updating. The selected model (either analytical or DL) provides backbone curves as input to the MCMC process.

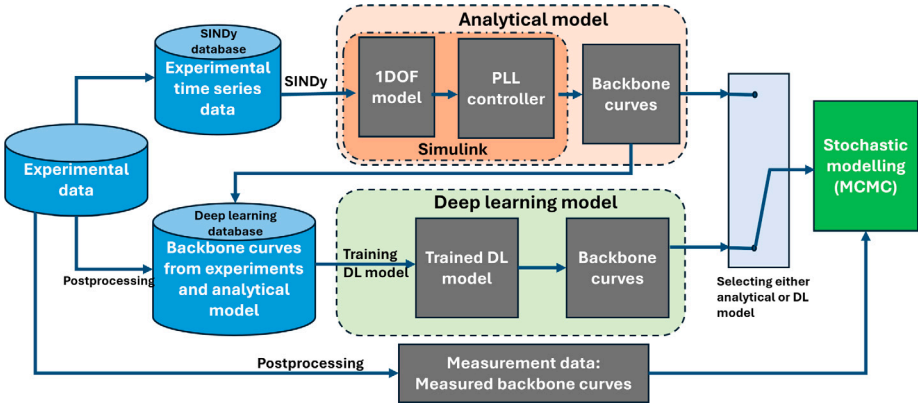

Fig. 1. Overall framework.

7. **Validation:** Measured backbone curves, obtained through postprocessing of experimental data, serve as the ground truth. These measured curves are used to validate the predictions from both the analytical and DL models. They also act as measurement data for the stochastic modelling process.

The key advantage of this framework is its flexibility and comprehensive approach. It combines physics-based modelling through the analytical model with data-driven techniques via the DL model. The stochastic modelling component accounts for uncertainties and variabilities in the system and the validation against experimental data ensures the reliability of the models. While this framework provides a robust theoretical foundation, its practical application and validation require careful experimental design and implementation, as detailed in the following section on the experimental setup.

3. Experimental setup

3.1. Methodology and approach

Thin panels are extensively utilised in sectors such as aviation, space exploration, and wind energy due to their excellent strength-to-weight ratios. These systems are particularly noted for their frictional contact and geometric nonlinearity. The use of mechanical fasteners such as pins, rivets, or bolts in panels leads to frictional behaviour at the joints. Additionally, the fixed boundaries of these panels lead to bending which results in membrane stretching or compression, thus influencing the overall bending stiffness. This interaction between bending and stretching is a significant instance of geometric nonlinearity in such structures.

In this study, a benchmark used by Malte et al. [31] in the Tribomechadynamics Research Challenge (TRC) is considered. The test setup comprises four primary components: a thin panel, a supporting structure, and two blades as shown in Fig. 2. The CAD model of the test setup, shown in Fig. 2, comprises four primary components: a thin curved panel, a robust supporting structure, and two blades securely fastened to both the blades and the columns using six M6 bolts with washers each side, arranged according to industry standards. The curved panel, with a thickness of 1.5 mm and length of 300 mm, is centrally positioned between the blades, simulating real-world conditions under dynamic loading. The blades are mounted on supports, which ensure structural stability while accommodating the panel's deformation during the test. The coordinate axes (x, y, z) provide spatial orientation, with x representing the length of the panel, y indicating its height, and z defining the depth.

In addition, the back plate is designed to be attached to the slip table of a substantial vibration system. Initially, the panel is perfectly flat. However, it is intentionally mounted at a slight angle of 2.2 degrees around the z-axis, with a 1.1-degree tilt on each side, causing the panel to adopt a curved shape once assembled. Complete CAD models, technical schematics, and detailed design documents, including setup guidelines, are given in a data repository [32]. This setup is designed to evaluate the panel's response under various loading conditions, with bolts and washers ensuring alignment and structural integrity. The TRC Benchmark system represents a standardised framework for analysing the behaviour of thin-walled structures under operational conditions, making it ideal for investigating vibration dynamics and structural resilience.

The benchmark used in this study represents a unique mix of geometric and contact nonlinearities, making the task of experimentally identifying the amplitude-dependent modal properties of the system complex. Consequently, shaker-based testing was employed, and the Phase Resonance Testing method (PRT) was utilised to analyse the nonlinear vibrational characteristics near a specific resonance. This technique relies on maintaining a constant phase lag between the response and the excitation, while gradually increasing or decreasing the excitation level [3-4]. A major benefit of this approach over traditional methods of nonlinear vibration testing (e.g. excitation-controlled testing) is its efficiency in generating fewer data points. This efficiency facilitates the precise tracking of the amplitude-dependent modal frequency, often referred to as the Backbone curve. Additionally, the modal damping ratio is derived from the equilibrium between the power dissipated and the power supplied on an average per cycle. To maintain the desired phase lag between the response and the excitation, phase control via feedback is essential. Typically,

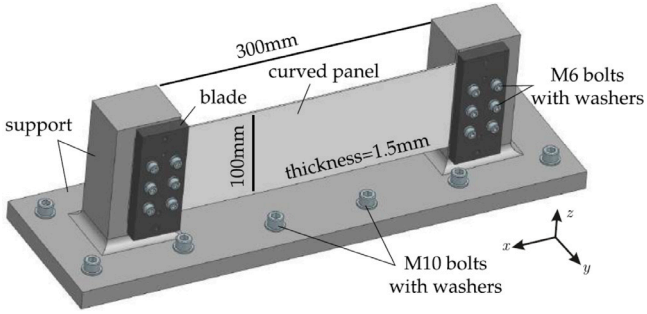

Fig. 2. TRC Benchmark system [31].

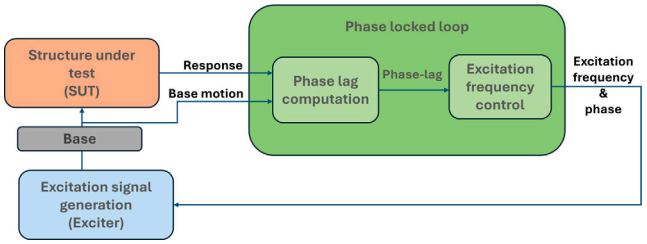

Fig. 3. Phase Resonant Testing approach.
Source: Inspired from [33].

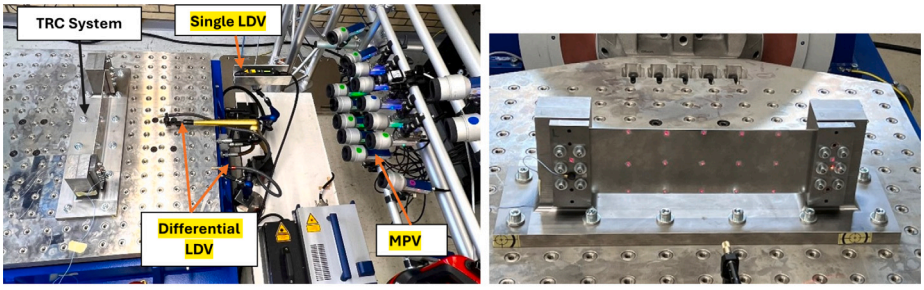

Fig. 4. TRC system (a) Test rig Instrumentation (b) TRC Benchmark.

this is achieved using a PLL, a common tool in the fields of electrical and control engineering [5-6]. However, a commercially available controller for such vibration testing is not yet available, necessitating a somewhat heuristic approach to tuning the control parameters.

Fig. 3 illustrates the Phase Resonant Testing approach to identify and sustain the resonant frequencies of a structure. The workflow begins with the Excitation Signal Generation (Exciter), which produces a controlled base motion applied to the SUT via a rigid base platform. The SUT's dynamic response, such as displacement or acceleration, is measured and fed into the Phase Lag Computation module. The Phase Lag Computation determines the phase difference between the base motion and the SUT's response, which is crucial for ensuring resonance. This information is processed within the Phase Locked Loop (PLL), where the Excitation Frequency Control dynamically adjusts the excitation signal's frequency and phase to align with the SUT's natural frequency. This feedback system ensures accurate tracking of resonance conditions, making it an invaluable tool for vibration testing.

3.2. Test rig and instrumentation

The benchmark system was constructed, assembled and tested during the Tribomechadynamics Research Camp, held from August 8th to September 9th, 2022. In the following, the instrumentation and the primary testing procedure are briefly summarised below. The in-depth description of the test sequences and further investigation outputs are provided in Arati et al. [32]. Test rig setup and detailed instrumentation are shown in Fig. 4(a).

The support structure is mounted on the slip table of a large shaker. Velocity measurements were taken at a point on the right blade using a single laser-Doppler vibrometer (LDV). Initial testing showed that the bottom plate, the pillars, and the blades

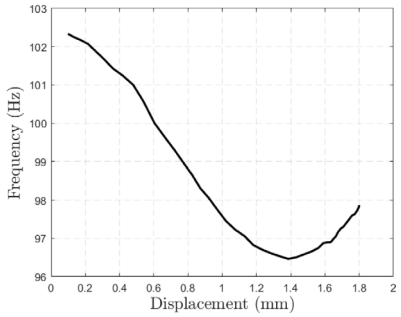

Fig. 5. One of the experimental backbone curves of the TRC system [31].

predominantly behave as a single rigid entity, moving in one specific direction. Consequently, this velocity was utilised as a benchmark for the base motion. At the centre of the panel, relative to the base, velocity was acquired using a differential LDV. A PLL is used to establish a phase resonance between the base velocity and the panel's response which incorporates synchronous demodulation to detect the phase. A proportional-integral controller is implemented to set the desired phase lag between the response and the excitation signal by adjusting the excitation frequency. A sinusoidal voltage signal, which varies over time in frequency and is set at a predetermined level, is fed to the shaker's amplifier. Once phase resonance is attained, the steady-state time series data is acquired. By gradually increasing and then decreasing the voltage signal gain, the backbone curve of the panel is constructed. These processes were conducted using a dSPACE MicroLabBox that operates with a 10 kHz sampling rate. To measure velocities at various points, a multi-point vibrometer (MPV) was employed, targeting 15 specific points arranged in a 5 by 3 grid on the panel as shown in Fig. 4(b). Reflective tape was placed at each measurement point to enhance the signal-to-noise ratio of the data collected.

3.3. Experimental backbone curves

Fig. 5 shows a sample of the tracked backbone curves using the described experimental approach. Fig. 5 shows a backbone curve with a strong nonlinearity present in the TRC system with the presence of softening and hardening behaviour in the panel due to the combination of dry frictional interactions in the joints and the geometric nonlinearity of the panel. The TRC panel is configured to allow the panel to arch, which leads to a softening effect as the structure deforms.

The experimentally derived backbone curves will be utilised as measurement data in stochastic modelling, focusing on the portion of the backbone curve up to approximately 0.9 mm displacement as shown in Fig. 5. It should be noted that while this region is referred to as "linear" for simplicity, the response is still nonlinear in nature. The time series data of this benchmark TRC system will be employed in SINDy for deterministic modelling, as proposed in the subsequent sections.

4. System identification using SINDy

SINDy is a novel data-driven technique for discovering governing equations and models directly from measurement data [28]. It leverages the sparse representation of non-linear dynamical systems to identify the most relevant terms and parameters that govern the system's behaviour. Unlike traditional system identification methods that rely on predefined model structures, SINDy operates on the principle that the governing equations of many physical systems can be expressed as sparse combinations of non-linear functions. By formulating the identification problem as a sparse regression task, SINDy can sift through libraries of candidate non-linear functions and select the most significant terms, discarding irrelevant or insignificant ones. This sparse modelling approach enables SINDy to extract parsimonious and interpretable models from high-dimensional data without prior assumptions about the form of the governing equations.

4.1. Methodology for applying SINDy to the experimental time series data

The velocity response from the MPV sensor at the centre point of the panel is used for system identification. Acceleration and displacement are computed from velocity data from the MPV sensor to simplify the analysis and ensure consistency and coherence in the data fed to the SINDy model. Utilising a single sensor's data for all required metrics avoids the potential inconsistencies and errors that could arise from combining measurements from different sensors, which may have varying accuracies, sensitivities, and response times. Thus, relying solely on the MPV data ensures a more reliable and streamlined process for system identification. Using the time series data from the MPV sensor, SINDy is employed to identify 1-DOF representation of the experimental setup. This simplified representation can provide insights into the system's dynamics and serve as a starting point for further analysis or model refinement. The remaining of this subsection describes the detailed procedure for identifying the 1-DOF model as shown in Fig. 6.

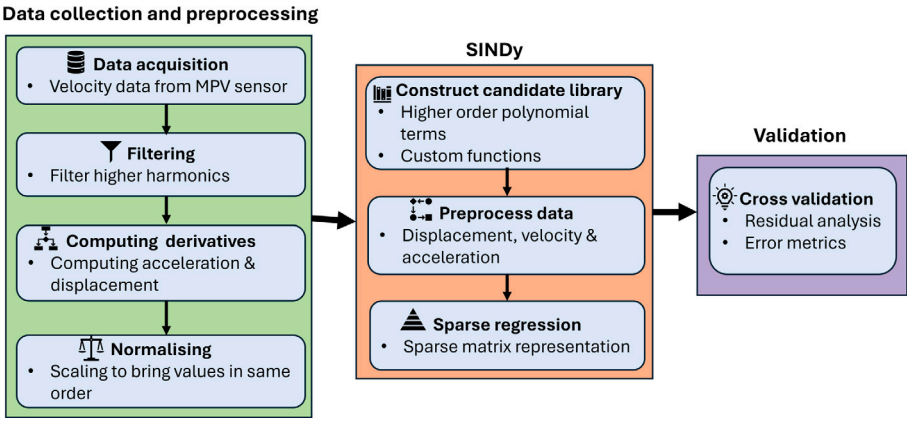

Fig. 6. SINDy framework.

4.1.1. Data collection and preprocessing

- **Velocity data collection:** The MPV sensor was chosen for its capability to provide high-resolution velocity measurements across multiple points simultaneously. This is particularly important for accurately capturing the dynamic response of complex structures like joint assemblies. The MPV system allows for detailed spatial resolution by measuring velocities at numerous points distributed over the surface of the panel. This comprehensive data collection facilitates a more precise analysis of the vibrational characteristics and mode shapes, which are critical for understanding the behaviour under different loading conditions. Additionally, the MPV sensor's non-contact nature eliminates potential interference with the system's dynamics, ensuring the integrity of the measurements [26].
- **Band-pass filtering:** In nonlinear dynamic systems, higher harmonics are crucial for accurately capturing behaviour and system parameters, especially in systems with strong nonlinearities like frictional contact interfaces [34]. Neglecting these harmonics can lead to significant errors. Therefore, it is essential to include higher harmonics in the system identification process for enhanced accuracy and reliability. Considering the first three higher harmonics is practical as it significantly improves parameter estimation accuracy while maintaining computational efficiency. These harmonics capture essential nonlinear characteristics such as non-linear stiffness, damping, and energy transfer mechanisms. Taghipour et al. [35] showed that considering three harmonics reduced the error in estimating nonlinear stiffness parameters to below 0.01%. Limiting to the first three harmonics keeps the computational burden manageable without sacrificing accuracy. To achieve this, a Butterworth band-pass filter is used to retain the first three harmonics, effectively isolating the primary frequencies of interest while removing unwanted higher harmonic noise.
- **Acceleration and displacement computation:** Acceleration and displacement are computed from the velocity data obtained from the MPV sensor using numerical methods to ensure consistency and coherence in the data fed to the SINDy model. Acceleration is calculated using the central difference method and the equation for acceleration $a(t)$ is given by Eq. (1)

$$a(t) \approx \frac{v(t+\Delta t) - v(t-\Delta t)}{2\Delta t} \tag{1}$$

where $v(t)$ is the velocity data and Δt is the time step between measurements.
Displacement is calculated using the trapezoidal rule, which approximates the integral of velocity over time. The equation for displacement $u(t)$ is given by Eq. (2):

$$u(t) \approx u(t_0) + \sum_{i=1}^{n} \left(\frac{v(t_i) + v(t_{i-1})}{2} \right) \Delta t \tag{2}$$

where $u(t_0)$ is the initial displacement, $v(t_i)$ and $v(t_{i-1})$ are the velocity values at the current and previous time steps, respectively, and Δt is the time step.
- **Data normalisation:** To ensure accurate and consistent input to the SINDy model, data scaling is performed on the displacement, velocity, and acceleration data. Each data type is divided by the maximum value observed in all the experimental data. This method of scaling has distinct advantages over conventional scaling techniques such as min–max scaling or standardisation. Min–max scaling adjusts data within a fixed range usually 0 to 1, which can distort the relationship between data points, especially in the presence of outliers or non-uniform data distributions. Standardisation transforms data to have a mean of zero and a standard deviation of one. This can obscure the physical significance of the data values and introduce biases, particularly if the data distribution deviates significantly from a normal distribution. By dividing each data type by its maximum value, we ensure that all values are scaled proportionally within a similar range.

$$\text{Scaled Value} = \frac{\text{Original Value}}{\text{Maximum Value}}$$

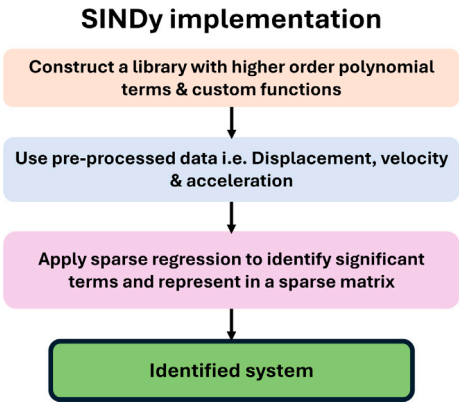

Fig. 7. Implementation steps of SINDy.

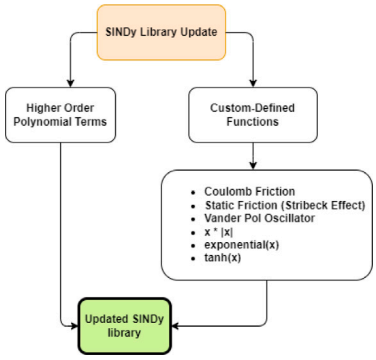

Fig. 8. Updated SINDy library.

4.1.2. SINDy algorithm implementation

SINDy is used to identify the governing equations of complex dynamic systems. It works by constructing a candidate library of potential terms that could describe the system's behaviour, then using preprocessed data it applies sparse regression techniques to pinpoint the most significant terms. This results in a simplified, yet accurate, representation of the system's dynamics in the form of a sparse matrix, facilitating a better understanding and analysis of the system's underlying mechanics. Fig. 7 illustrates the implementation steps of the SINDy method, which involves constructing a function library, using pre-processed dynamic data, applying sparse regression to identify significant terms, and deriving a simplified system model.

- **Construction of a candidate library:** Along with higher order polynomial terms, to enhance the accuracy of the system identification process, the SINDy library is updated with custom-defined functions that better accommodate the effects of friction and contact, which significantly influence the behaviour of jointed structures. The customised SINDy library as shown in Fig. 8 includes: Coulomb friction, which models the constant dry friction force after overcoming static friction, capturing the behaviour of sliding surfaces in contact; the static friction or Stribeck effect function, which accounts for increased friction force at low sliding velocities; the Vander Pol oscillator, a non-linear function that captures self-excited vibrations and limit cycle behaviour due to friction and contact interactions; the $x \cdot |x|$ term, which represents non-linear, asymmetric behaviour from directional contact and friction forces; the exponential(x) function for modelling potential non-linear growth or decay in the system's response; and the tanh(x) function, a smooth non-linear function that models saturation effects or bounded behaviour in the system's dynamics.
- **Using preprocessed data:** SINDy relies on preprocessed data to accurately identify the dynamics of the system. The preprocessed data includes displacement, velocity and acceleration out of which velocity is captured from the sensor and displacement and acceleration is computed from velocity data.
- **Application of sparse regression:** In the SINDy algorithm, sparse regression is applied to identify significant terms that contribute to the system's dynamics. Using sequential thresholding, the algorithm selectively identifies the most influential terms from the candidate library. This process filters out less relevant terms, focusing only on those that significantly impact the system's behaviour. The identified significant terms are then represented in a sparse matrix format, which efficiently captures the essential dynamics of the system while reducing computational complexity. This approach ensures that the resulting model is both parsimonious and accurate, facilitating better understanding and prediction of the system's behaviour.

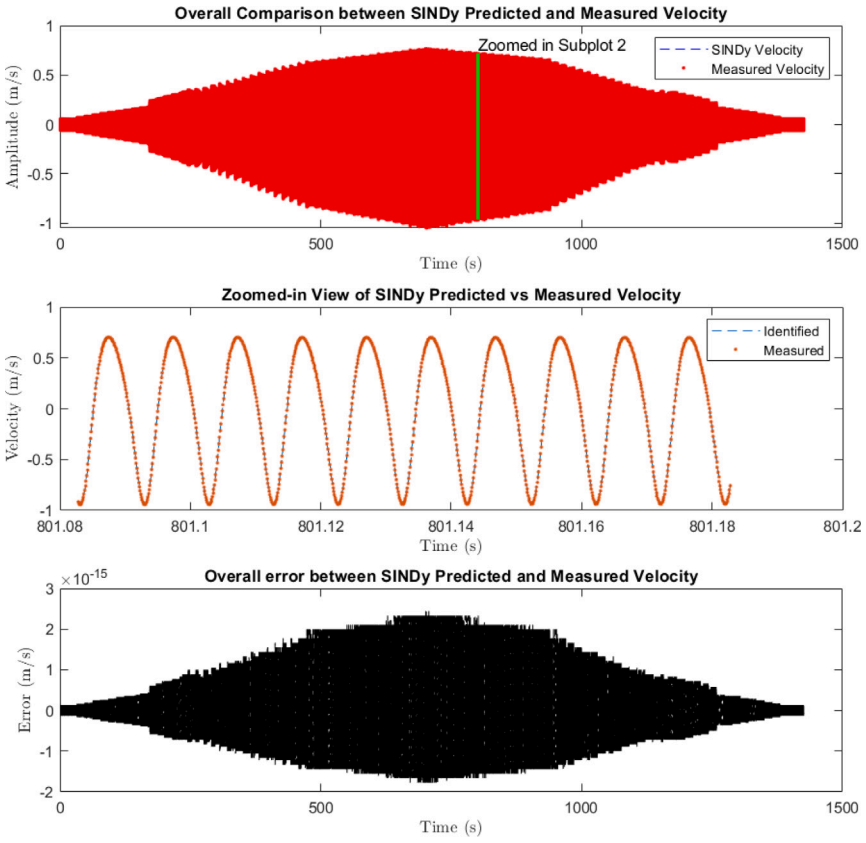

Fig. 9. Comparison of SINDy predicted and measured velocity. Top: Overall comparison showing the full-time range. Middle: Zoomed-in view highlighting the close agreement between identified and measured velocities over a short time interval. Bottom: Overall error between SINDy predicted and measured velocity.

The experimental bolted plate system, being a continuous structure, inherently possesses multiple degrees of freedom. However, for the primary vibration mode of interest, the system's behaviour can be effectively approximated using an equivalent Single Degree of Freedom (SDOF) model. In this equivalent SDOF representation, x denotes the displacement at the centre of the plate, and f represents base excitation. This simplified model captures the essential dynamics of the first mode while maintaining mathematical tractability.

The SINDy identified 1-DOF model is represented in Eq. (3). The most dominant terms, which capture the essential dynamics of the system, are shown in this equation. These terms were selected based on their significant contribution to the system's behaviour, as determined by the sparse regression process.

$$\begin{aligned}&\ddot{x} + k_1 x + k_2 \dot{x} - k_3 x^2 - k_4 x\dot{x} + k_5 \dot{x}^2 - k_6 x^3 - k_7 x\dot{x}^2 \\ &\quad -k_8 \dot{x}^3 - k_9 x|x| + k_{10}\dot{x}|\dot{x}| + k_{11}(1 - k_{12}x^2)\dot{x} = f\end{aligned} \tag{3}$$

$k_1 = 4.49 \times 10^5$ N/m $\quad k_2 = 1.85$ Ns/m $\quad k_3 = 2.60 \times 10^7$ N/m^2

$k_4 = 2.95 \times 10^4$ Ns/m^2 $\quad k_5 = 60.5$ Ns^2/m^2 $\quad k_6 = 3.32 \times 10^9$ N/m^3

$k_7 = 2.33 \times 10^4$ Ns/m^3 $\quad k_8 = 9.50$ Ns^3/m^3 $\quad k_9 = 3.35 \times 10^7$ N/m^2

$k_{10} = 11.6$ Ns^2/m^2 $\quad k_{11} = 5.66$ Ns/m $\quad k_{12} = 5.10 \times 10^5$ m^{-2}

4.1.3. Validation

The SINDy identified model's accuracy was validated by comparing its predictions with experimental data. The comparison was performed for both velocity and acceleration responses. The overall comparison between the SINDy predicted and measured velocity is shown in Fig. 9. The top subplot displays the full velocity response, while the middle subplot provides a zoomed-in view over a short time interval, allowing for a more detailed examination of the predicted and measured velocity. The bottom subplot shows the error between the SINDy predicted and measured velocity over the entire time range.

The residuals appear to be centred around zero, with some spikes or deviations at certain time points. The low mean error (−4.7427e−20), maximum error (2.4425e−15), and root mean squared error (RMSE) (8.4667e−16) indicate good overall agreement between the predicted and measured velocity.

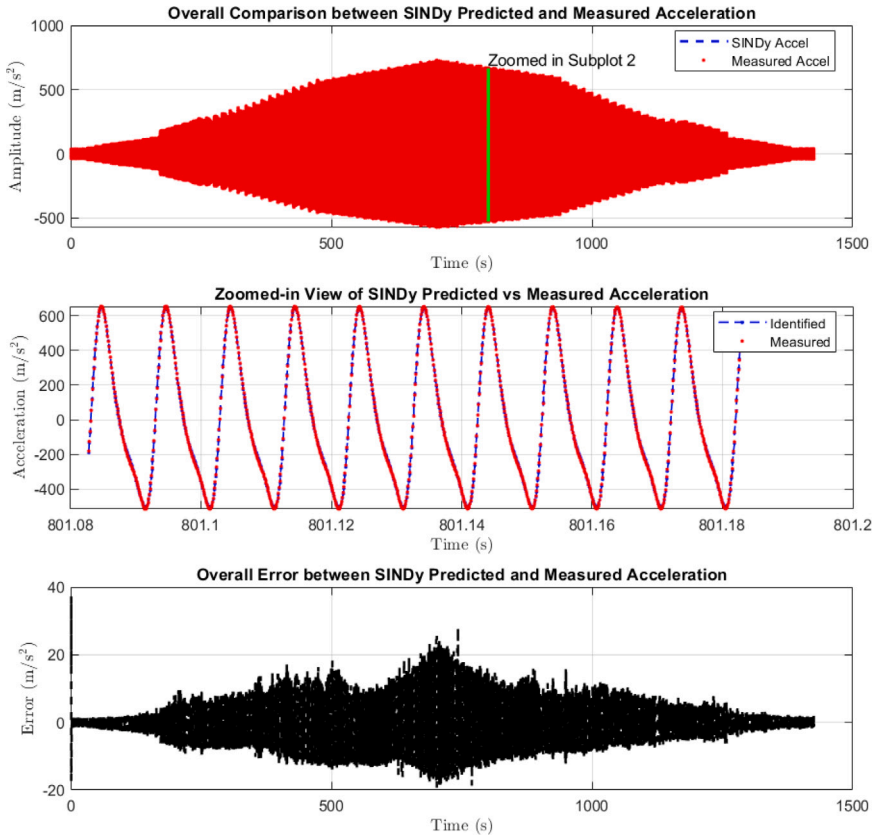

Fig. 10. Comparison of SINDy predicted and measured acceleration. Top: Overall comparison showing the full-time range. Middle: Zoomed-in view highlighting the close agreement between identified and measured accelerations over a short time interval. Bottom: Overall error between SINDy predicted and measured acceleration.

Similarly, Fig. 10 presents the overall comparison between the SINDy predicted and measured acceleration. The subplots follow the same arrangement as the velocity comparison, with the top subplot displaying the full acceleration response, the middle subplot providing a zoomed-in view, and the bottom subplot showing the error between the SINDy predicted and measured acceleration.

The residuals exhibit a distinct pattern, with larger deviations occurring during high acceleration regions, indicating potential model limitations in capturing the nonlinearities during those periods. The larger mean error (−4.3484e−05), maximum error (0.051254), and RMSE (0.0052219) compared to the velocity metrics suggest less accurate predictions for acceleration.

While the errors are significant, it is essential to consider the range of variation in the acceleration data. The acceleration response spans a wide range, with peak values reaching approximately $600\,\mathrm{m/s^2}$. The observed errors, although not negligible, may still be acceptable for the purpose of system identification, particularly if the primary focus is on capturing the overall dynamics and behaviour.

In SINDy, velocity estimates typically exhibit lower error than acceleration estimates. This discrepancy can be attributed to the fact that acceleration, being the second derivative of position, is more susceptible to noise amplification and numerical differentiation errors. Additionally, the sampling rate and measurement precision of the original data often prove sufficient for velocity estimation but may fall short of accurate acceleration determination. These factors collectively contribute to the generally higher accuracy of velocity terms compared to acceleration terms in SINDy models.

Despite the larger errors during high acceleration regions, the identified model demonstrates its ability to reasonably approximate the acceleration response across the entire time range. This capability can serve the purpose of system identification, providing valuable insights into the system's dynamics and enabling further analysis or refinement of the model if higher accuracy is required for specific applications or regions of interest. After establishing the SINDy model's capability to approximate the system's dynamics, the focus has now turned to integrating this identified model with the PLL method to further enhance understanding of the system's nonlinear behaviour and extract its backbone curve.

5. SINDy identified 1-DOF model integration with PLL: Analytical model

The PLL method is utilised in this work to generate the backbone curve of the nonlinear dynamic system under investigation. This method employs feedback control to track a sequence of points along the phase resonant backbone curve, enabling the identification

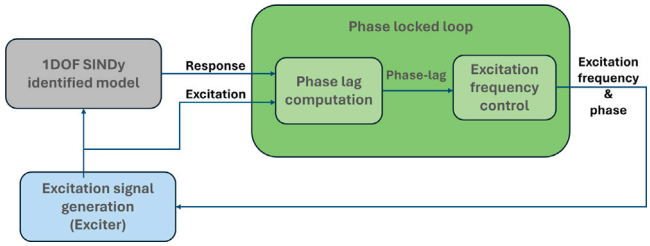

Fig. 11. Analytical model: PLL on the 1-DOF model in Simulink.

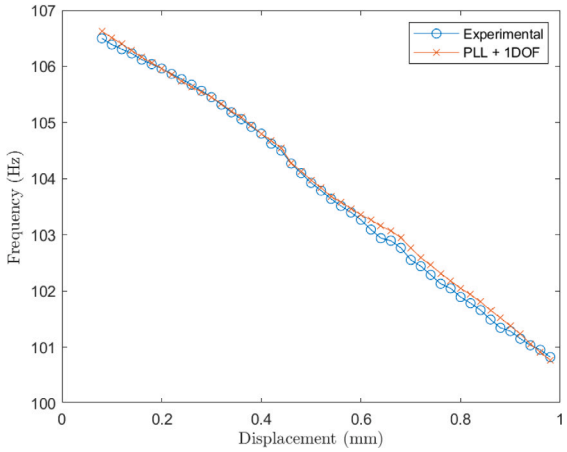

Fig. 12. Comparison of the experimental and analytical model backbone curves.

of modal properties from the periodic steady-state response. Feedback control is more convenient and robust than manual tuning, as it automatically adjusts the system to track phase resonant points along the backbone curve. The PLL generates a sinusoidal signal that is fed into the exciter, with the control loop continuously adjusting the oscillation frequency until phase resonance is achieved. Depending on whether displacement, velocity, or acceleration is measured, the target phase must be adjusted accordingly: −90° for velocity, 0° for displacement, and +90° for acceleration. This phase adjustment ensures that the system remains in a phase resonant state throughout testing, providing accurate and reliable modal properties.

In this study, the SINDy identified 1-DOF model is integrated with the PLL controller in a Simulink environment. The PLL controller is implemented as a feedback control loop that continuously adjusts the excitation frequency to maintain phase resonance with the SINDy-identified model's response as shown in Fig. 11.

Fig. 12 illustrates the comparison by plotting the frequency (Hz) against displacement (mm) (i.e. the backbone curves) for both the experimental data and the analytical model identified using the PLL + 1-DOF approach. The two curves are closely aligned across the entire range of displacements, indicating that the analytical model accurately captures the system's dynamics. There are minor deviations between the experimental data and the analytical model, which are expected due to experimental uncertainties and simplifications in the analytical model. The difference in the backbone curves, despite negligible velocity error, likely arises from factors such as unmodelled higher-order nonlinearities, slight parameter mismatches in the SINDy model, and small phase-tracking errors in the PLL. Experimental noise, boundary condition variations, and coupled degrees of freedom could also contribute. Additionally, numerical discretisation in the analytical model may deviate from the continuous experimental setup. These small discrepancies collectively influence the backbone curve despite accurate velocity predictions. However, running the analytical model to obtain one backbone curve was found to be computationally exhaustive, leading to the development of a deep learning model for computation optimisation.

6. Deep learning model for computation optimisation: DL model

The analytical model developed by integrating the SINDy-identified 1-DOF model with the PLL controller in Simulink is computationally expensive, especially when performing simulations or analyses over extended time periods or under various parameter configurations. The computational complexity arises from the need to solve the governing nonlinear differential equations at each time step, which can be particularly demanding for systems with intricate nonlinearities. Using this analytical model in a Bayesian analysis framework, such as MCMC, would further add to the computational cost, as the Bayesian approach requires repeated evaluations of the model to sample the parameter space.

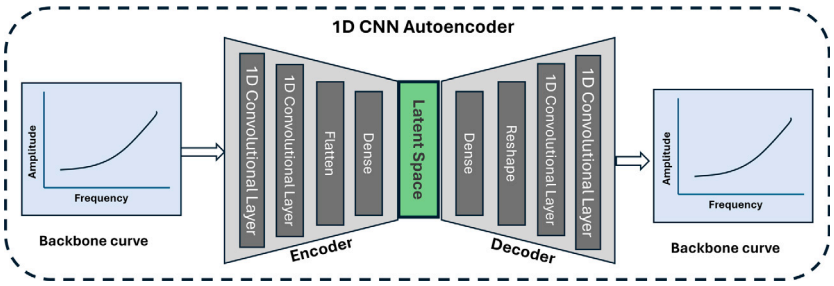

Fig. 13. Training phase: Deep Learning models for computation optimisation. 1D CNN Autoencoder.

Table 1
Autoencoder model parameters.

Component	Layer Type	Parameters
Input Layer	Input	Shape: $(41, 2)$
Encoder Output	Encoder	Shape: $(64,)$
Decoder Output	Decoder	Shape: $(41, 2)$
Loss Function	Loss	Mean Squared Error (MSE)
Optimiser	Optimiser	Adam, Learning Rate: $1e^{-4}$
Metrics	Evaluation	Pearson Correlation

Table 2
Encoder parameters.

Layer	Layer type	Parameters
Input Layer	Input	Shape: $(41, 2)$
Conv1D Layer 1	Conv1D	Filters: 64, Kernel Size: 5, Padding: 'same', Activation: 'elu'
Conv1D Layer 2	Conv1D	Filters: 32, Kernel Size: 5, Padding: 'causal', Activation: 'elu', Dilation Rate: 4
Flatten Layer	Flatten	–
Dense Layer	Dense	Units: 64, Activation: 'relu'

Deep learning, with its ability to approximate complex nonlinear functions efficiently, presents an opportunity to reduce this computational burden. By training a deep neural network to learn the underlying dynamics of the system from the analytical model, it becomes possible to replace the computationally intensive numerical integration with a highly optimised inference process on the trained neural network. Furthermore, to enhance the robustness and generalisation of the DL model, it is trained not only on the experimental data but also on data generated from the analytical model. This combined training approach leverages the strengths of both the analytical and data-driven models, allowing the DL model to capture the complex system dynamics while benefiting from the additional information provided by the analytical model.

6.1. Architecture and training process of the DL model

Two DL models are used in the training phase for computation optimisation as shown in Figs. 13 and 14 illustrates the training phase of deep learning models for computational optimisation, showcasing Fig. 13, the 1D CNN Autoencoder (see Tables 1–3 for model parameters) for feature extraction and reconstruction, and Fig. 14, the Feedforward Neural Network (FFNN) for latent space mapping (see Table 4 for model parameters). The autoencoder is used for the dimensionality reduction of the backbone curves, and the dimensionally reduced latent space representations are then utilised as target outputs to train the neural network model.

- **1D Convolutional Neural Network (CNN) Autoencoder:** The 1D CNN model takes backbone curves as input, which are frequency-domain representations. The encoder part of the autoencoder compresses the input backbone curves into a lower-dimensional latent space representation while preserving the most important features and characteristics. This latent space is the dimensionally reduced form of the input data.
- **Feed Forward Neural Network (FFNN):** The FFNN model takes system parameters as input and aims to predict the corresponding backbone curves. To achieve this, the FFNN is trained using the latent space representations obtained from the 1D CNN Autoencoder as targets. By learning the mapping from system parameters to the latent space, the FFNN can effectively generate the backbone curves as output for new system parameter inputs.

This two-stage approach allows the FFNN to learn the relationship between system parameters and the corresponding backbone curves efficiently, leveraging the compressed representations from the 1D CNN Autoencoder.

Table 3
Decoder parameters.

Layer	Type	Parameters
Input Layer	Input	Shape: (64,)
Dense Layer	Dense	Units: 1312, Activation: 'relu'
Reshape Layer	Reshape	Target Shape: (41, 32)
Conv1D Layer 1	Conv1D	Filters: 64, Kernel Size: 5, Padding: 'causal', Activation: 'elu', Dilation Rate: 4
Conv1D Output	Conv1D	Filters: 2, Kernel Size: 5, Padding: 'same', Strides: 1

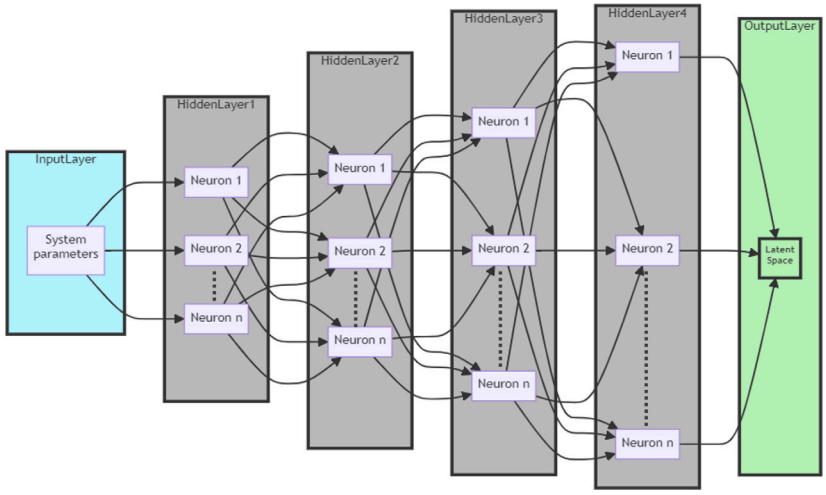

Fig. 14. Training phase: Deep Learning models for computation optimisation. Feed Forward Neural Network.

Table 4
FFNN model parameters.

Component	Layer Type	Parameters
Input Layer	Input	Shape: (12,)
Hidden Layer 1	Dense	Units: 512, Activation: 'elu'
Hidden Layer 2	Dense	Units: 512, Activation: 'elu'
Hidden Layer 3	Dense	Units: 512, Activation: 'elu'
Hidden Layer 4	Dense	Units: 512, Activation: 'elu'
Output Layer	Dense	Units: 64, Activation: None
Optimiser	Adam	Learning Rate: $1e^{-3}$
Loss Function	Calculation	Mean Squared Error
Metrics	Evaluation	Pearson Correlation

In the prediction phase as shown in Fig. 15, the trained FFNN model is combined with the decoder part of the 1D CNN Autoencoder to generate the final backbone curve predictions. During the prediction phase, the following steps are performed:

- The FFNN model takes the new system parameters as input.
- The FFNN outputs the predicted latent space representation corresponding to the input system parameters. This latent space representation is the dimensionally reduced form learned during the training phase.
- The decoder part of the 1D CNN Autoencoder is then applied to the predicted latent space representation from the FFNN.
- The decoder upsamples and reconstructs the predicted latent space representation to generate the final predicted backbone curve in the original frequency-domain representation.

The prediction phase combines the FFNN's ability to map system parameters to the latent space and the decoder's ability to reconstruct the latent space representation back into the original backbone curve format. This approach leverages the strengths of both models: the FFNN learns the complex mapping from system parameters to the compressed latent space, while the decoder handles the reconstruction of the latent space into the final backbone curve format.

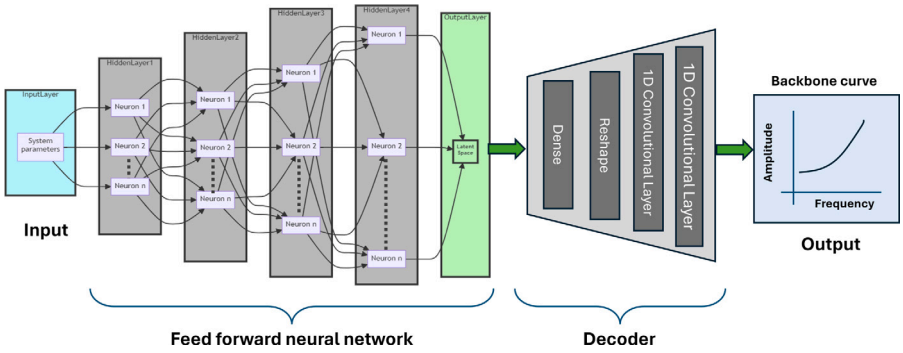

Fig. 15. Prediction phase.

Table 5
Performance of the model across different dataset sizes.

Datasize	Ratio	MSE	MAE	MAPE
200	7	2.82×10^{-5}	0.00282	0.774
300	11	2.72×10^{-5}	0.00274	0.924
400	15	2.42×10^{-5}	0.00271	1.502
500	19	1.21×10^{-5}	0.00239	0.729

6.2. Results from DL modelling

The deep learning (DL) model for predicting backbone curves was trained using a mixed dataset composed of both experimental and analytical model data. Given the importance of dataset composition, a systematic analysis was conducted to investigate the effect of dataset ratio on model validation results. The training dataset consisted of:

- **Experimental data:** 25 samples
- **Analytical model data:** Varied from 175 to 475 samples, depending on the total dataset size

The dataset ratio is defined as:

$$\text{Dataset Ratio} = \frac{\text{Datasize} - 25}{25} \tag{4}$$

where *Datasize* represents the total number of training samples. To evaluate the effect of dataset ratio on model accuracy, the DL model was trained using dataset sizes of 200, 300, 400, and 500 samples, corresponding to dataset ratios of 7, 11, 15, and 19, respectively. Table 5 presents the model's performance metrics across different dataset configurations. The Mean Squared Error (MSE), Mean Absolute Error (MAE), and Mean Absolute Percentage Error (MAPE) were used to evaluate model performance.

It is worth noting that the improvement in performance metrics becomes increasingly marginal as the dataset size grows from 200 to 500 samples. While further expansion of the dataset size might yield additional improvements, these potential gains must be weighed against the increased computational costs and training time. For the specific application of predicting backbone curves, the accuracy achieved with 500 samples (dataset ratio of 19) appears to provide an optimal balance between model performance and computational efficiency. During this analysis, the model was retrained to ensure consistency across different dataset sizes. This resulted in a slight variation in the MSE value of the current case (1.21×10^{-5}) as compared to the MSE value of the final trained model (5.119×10^{-6}) for the same dataset ratio. This variation can be attributed to the stochastic nature of deep learning training, including differences in weight initialisation and data shuffling. However, the new MSE remains within an acceptable range, maintaining strong model performance without affecting the study's overall conclusions.

The performance of the DL model is evaluated based on its ability to predict the backbone curves from system parameters. The model was trained using 500 samples out of which 25 were measured from the experiments described in Section 2 and the remaining were from the analytical model described in Section 4. The six plots displayed in Fig. 16 represent randomly drawn cases from the 100 test cases. Each subplot compares the predicted backbone curves with the experimental ones. The close alignment of the predicted and actual data points across all plots demonstrates the model's robustness and generalisability.

The time required to predict 100 samples was measured at 0.4073 s. This highlights the efficiency of the DL model, making it suitable for real-time applications and scenarios requiring faster simulations. The MSE between the predicted and actual values was calculated to be 5.119×10^{-6} mm^2. This low error value indicates a high degree of accuracy in the model's predictions. The Pearson correlation coefficient was found to be 0.9975, indicating an excellent linear relationship between the predicted and actual values. This high correlation further validates the model's predictive capabilities. The model consistently predicts the backbone curves accurately when provided with system parameters, confirming its reliability and precision. Building on these capabilities, the next section explores stochastic model updating using both the analytical model and the DL model.

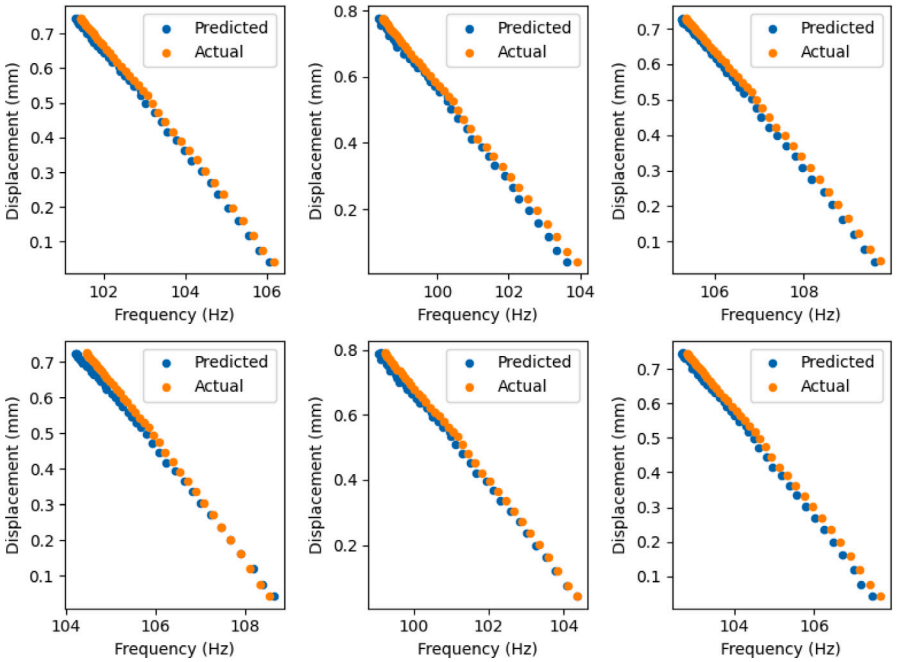

Fig. 16. Prediction results: Predicted (blue circles) and experimental backbone curves (orange circles). (For interpretation of the references to colour in this figure legend, the reader is referred to the web version of this article.)

7. Stochastic model updating using DL model

In this section, the process of stochastic model updating using a deep learning model is explained. The DL model combines a feed-forward neural network and a 1D CNN decoder, trained to generate the backbone curve from system parameters. This section investigates the stochastic model updating of the system using the DL model, leveraging MCMC within Bayesian framework methods to account for uncertainties.

Bayesian inference is a statistical framework that updates the beliefs about the distribution of parameters in a system based on observed data using Bayes' Rule. It involves three key components: the likelihood function, representing the probability of observing the data given specific parameter values; the prior distribution, representing the initial beliefs about the parameters before observing any data; and the posterior distribution, which combines the prior and the likelihood in accordance with Bayes' Rule. Mathematically, the posterior distribution is expressed as

$$P(\boldsymbol{\Theta}|D,M) = P(D|\boldsymbol{\Theta},M)\cdot P(\boldsymbol{\Theta}|M)/P(D|M) \tag{5}$$

where $\boldsymbol{\Theta}$ is the parameter vector, D is the observed data, and M is the system model. For practical purposes, Bayesian inference involves computing the posterior distribution for candidate parameter values and using this to infer the most likely parameter values. For detailed insights into Bayesian inference, readers can refer to foundational papers on Bayesian inference for stochastic modelling in structural dynamics [6,7,14,36–40]. In this study, a uniform prior distribution for each system parameter with defined bounds is assumed. The product of likelihood and prior for posterior calculation is taken, using backbone curves as measurement data.

This study leverages the likelihood function introduced by Pandey et al. [30] for simultaneously updating both linear and non-linear parameters of a non-linear dynamical system, employing standard Bayesian inference to calculate the parameter distributions based on observed data. Fig. 17 represents the likelihood function, showing the transformation of backbone curves into individual probability distribution functions and their combination into a joint probability distribution function. The likelihood function is constructed through specific points along backbone curves at different amplitudes, forming a joint distribution across amplitudes. The red dots in Fig. 17 illustrate these points and the resulting likelihood function.

The study employs MCMC, specifically the Metropolis–Hastings (MH) algorithm, to develop a stochastic model for system parameters using measurement data to establish the Bayesian likelihood function. For a comprehensive understanding of MCMC or the application of MCMC for stochastic modelling in structural dynamics, readers can refer to papers [41–44]. Traditional Bayesian methods face challenges with non-linear stochastic dynamic systems due to complex likelihood functions and sensitivity to initial conditions. The proposed approach mitigates these issues by combining MCMC with a likelihood function approximation using backbone curves, simplifying the representation of system dynamics, reducing complexity, and enhancing robustness against model misspecification and data limitations [30].

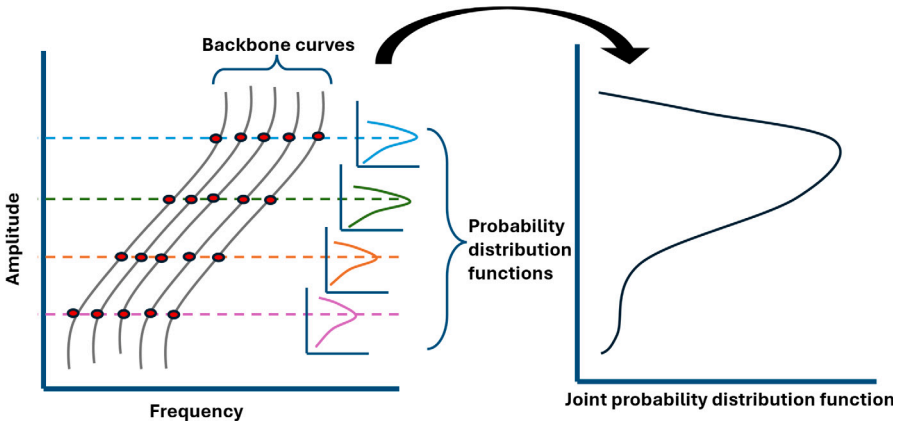

Fig. 17. Likelihood function.

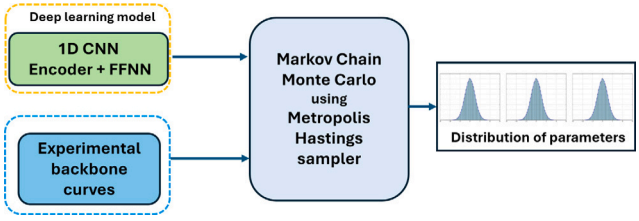

Fig. 18. Stochastic model framework using DL model.

7.1. MCMC for stochastic modelling using DL model

The DL model described in Section 6 is used within the MCMC framework as shown in Fig. 18. Fig. 18 illustrates a stochastic model framework that utilises a deep learning model to generate experimental backbone curves, which are then input into a Markov Chain Monte Carlo sampling process for uncertainty quantification. This DL model, a combination of a 1D CNN Encoder and an FFNN, is utilised to generate backbone curves for a set of system parameters. This approach replaces the analytical model to save computation time, leveraging the efficiency and predictive power of DL. The 1D CNN Encoder extracts essential features from the data, while the FFNN processes these features to predict the system's backbone curves.

By integrating the DL-generated backbone curves and experimental data, the MCMC process develops a robust stochastic model of the system parameters. The MH sampler iteratively refines the parameter estimates, sampling from the posterior distribution based on the information provided by both the DL model and experimental backbone curves. This method not only enhances computational efficiency but also ensures that the stochastic model accurately reflects complex system dynamics, combining machine learning techniques with experimental data to provide a comprehensive understanding of parameter distributions.

7.1.1. Results from MCMC sampling using DL model

Using the DL model, MCMC sampling attained an acceptance rate of 0.06 with a computation time of around 11 min for 30000 MCMC samples. The scatter plots in Fig. 19 illustrate the distribution of 30,000 MCMC samples for system parameters using a DL model, divided into two 6×6 matrices for better visualisation. The first matrix, which includes parameters k_1 to k_6, shows diagonal histograms representing the marginal distributions of each parameter. The second scatterplot matrix, which includes parameters k_7 to k_{12}, follows a similar pattern. The marginal distributions for these parameters also show varying degrees of variability, with few parameters exhibiting narrower distributions and few showing wider distributions.

The marginal distributions (diagonal) depict the distribution of individual parameters. Most distributions appear to be unimodal, with a single peak, which suggests that the MCMC sampling has likely converged well and represents a single mode of the posterior distribution. The width of the distributions indicates the uncertainty in the estimation of each parameter. Narrow distributions suggest that the parameter estimates are more precise, while wider distributions indicate greater uncertainty. The scatter plots for most parameter pairs exhibit cloud-like shapes, which indicate that the parameters are sampled from regions with high joint probability densities. These clouds are mostly centred, which is typical for well-behaved MCMC sampling where the samples are concentrated around the posterior. Some plots show a more elliptical shape, which may suggest that there is some linear or non-linear relationship between the parameters.

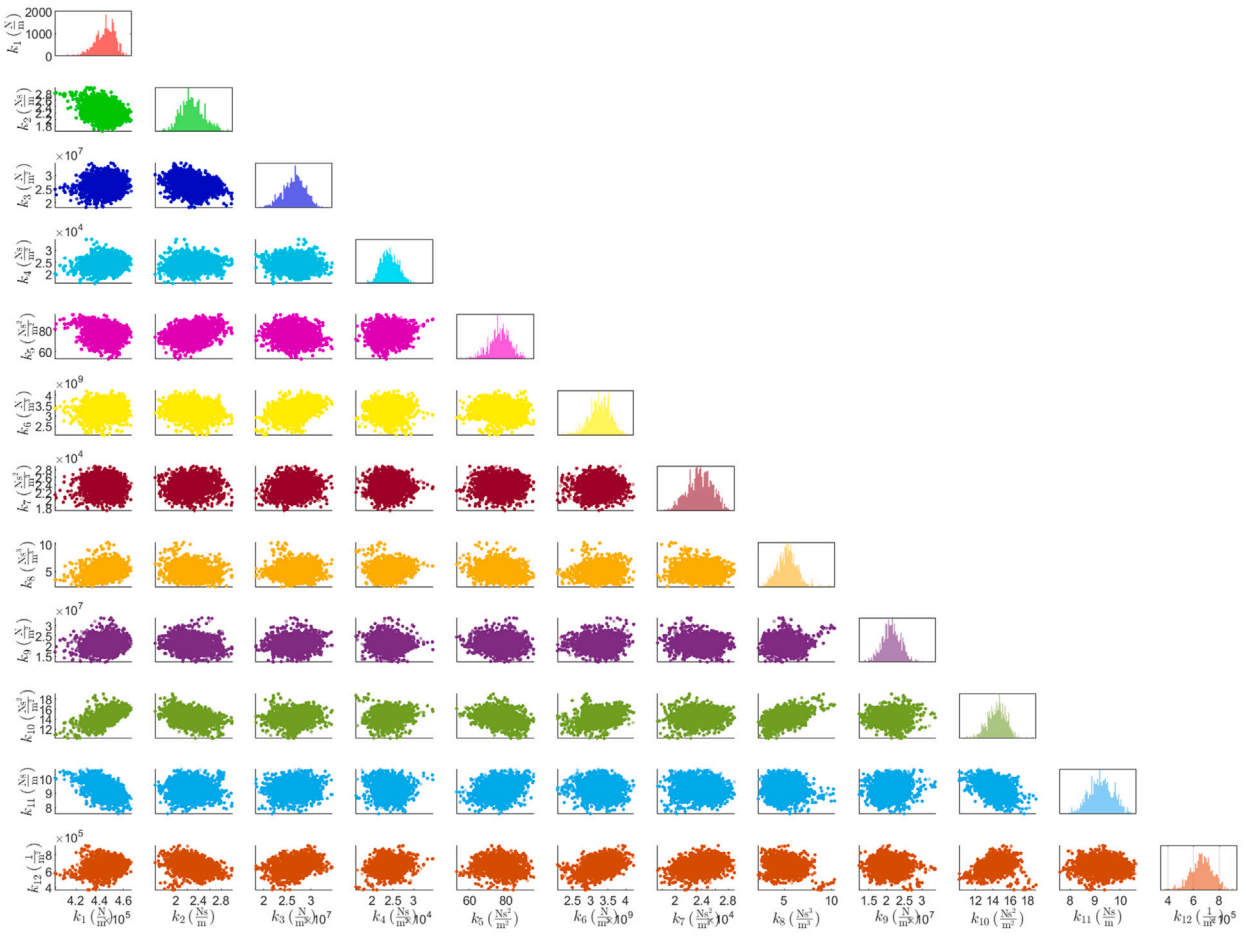

Fig. 19. Scatterplot of MCMC samples using DL model for parameters k_1 to k_{12}.

7.1.2. Correlation between MCMC samples

The correlation plot in Fig. 20 visualises the pairwise relationships between 12 parameters obtained through MCMC sampling using a DL model. Each square in the plot represents the correlation between two parameters. The colour intensity and direction (red or blue) indicate the strength and direction of the correlation. The diagonal elements of the plot (where the parameter index matches on both axes) show the autocorrelation of each individual parameter, which is 1.0 in all cases, as expected. The off-diagonal elements show the cross-correlations between different parameters. Strong positive correlations (close to 1.0) are shown in red. Strong negative correlations (close to −1.0) are shown in dark blue. Weak or negligible correlations (close to 0.0) are shown in light colours (yellow, green, and cyan). The correlation pattern suggests that the parameters are not entirely independent of each other.

Some of the parameters such as (k_1, k_{10}), (k_3, k_6) and (k_8, k_{10}) exhibit a strong positive correlation suggesting that as one of these parameters increases, the other tends to increase as well. This might indicate that these two parameters could be influencing the same aspect of the model or are related in a way that a change in one directly impacts the other. Parameters such as (k_1, k_{11}) and (k_2, k_{10}) have strong negative correlations hinting at a possible interaction or dependency between them within the model. Several parameter pairs have correlations close to zero, indicating no linear relationship. For example, correlations involving (k_7) with most other parameters are weak, suggesting that (k_7) might be more independent or unrelated to those parameters in the model. The overall correlation structure provides insights into the complex interactions and dependencies between the 12 parameters. The high correlations between the parameters could suggest potential collinearity or redundancy in the model parameters. This could imply that the model might be over-parameterised. Strong correlations may indicate that certain parameters are closely tied to specific dynamics or constraints within the system modelled by the DL (Deep Learning) approach.

7.1.3. Comparing MCMC sampled backbone curves with experimental curves

Fig. 21 shows the measured backbone curves and the backbone curves from MCMC samples using the DL model. Measured backbone curves may exhibit unusual behaviour due to external influences such as configuration variability or reassembly differences during the experiment. Specifically, in Fig. 21(a), two prominent backbone curves stand out, which are likely linked to the

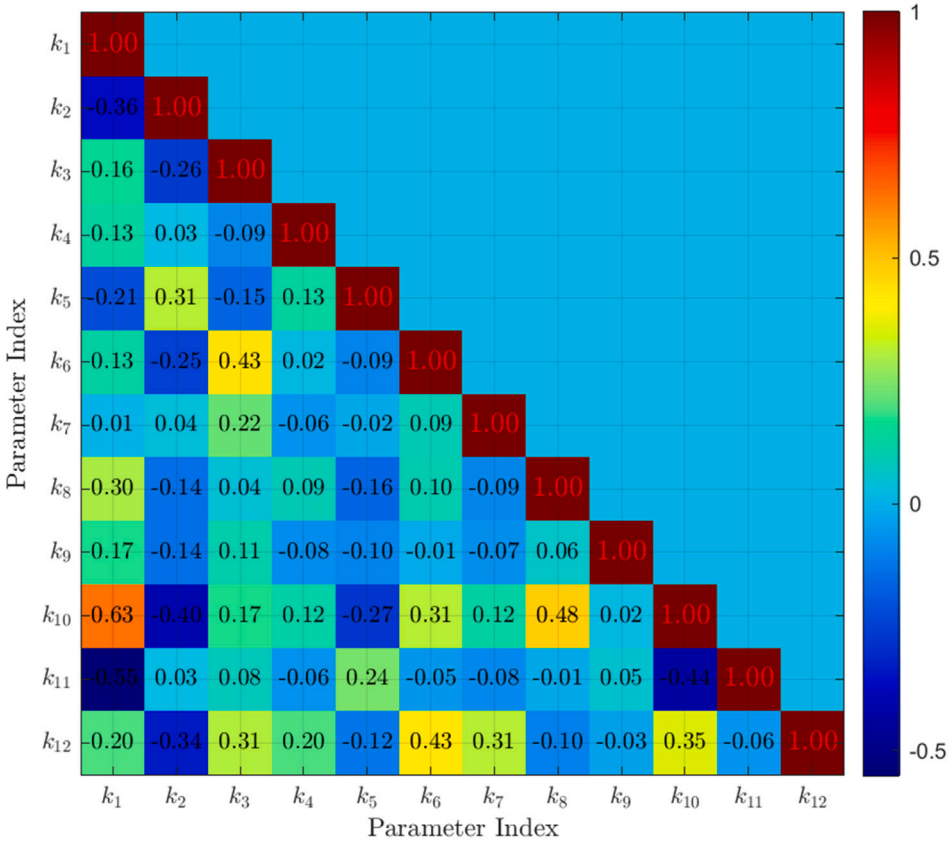

Fig. 20. Correlation matrix of MCMC samples.

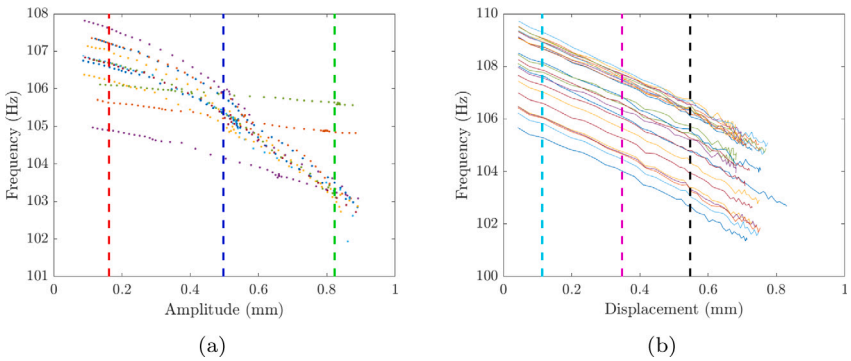

Fig. 21. (a) Measured backbone curves (b) MCMC sampled backbone curves.

configuration involving the heat-treated panel from TRC 2022. This heat treatment may alter the structural dynamics or introduce variability that is not accounted for in the analytical model used for sampling. The low, mid, and high amplitude levels are marked red, blue, and green in Fig. 21(a) and cyan, magenta, and black in Fig. 21(b).

The PDFs are compared at different amplitude levels to evaluate the model's capability in capturing the system's nonlinear behaviour across its operational range. To ensure a reliable representation of the distribution, the fitmethis [45] MATLAB function is used to determine the best-fitting distribution among all available distributions in MATLAB. It is well known that generating a large number of experimental datasets is expensive. Therefore, this approach helps mitigate the challenges associated with small

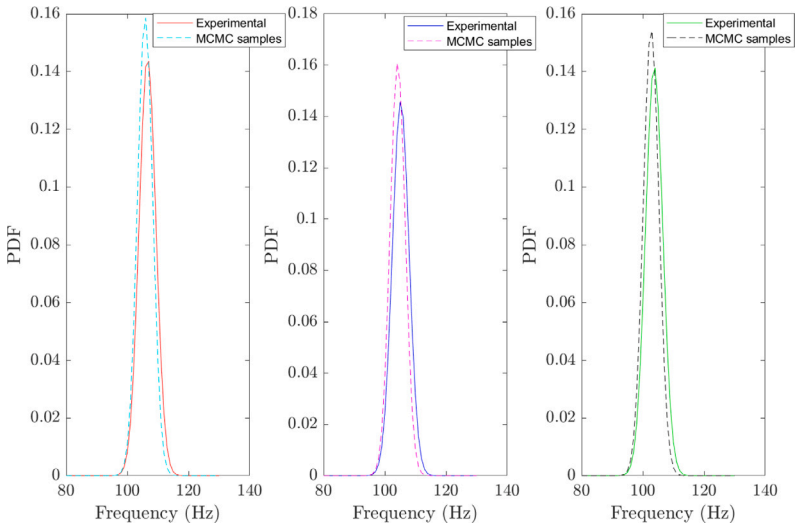

Fig. 22. PDF comparison for three amplitude levels: low, mid and high (left to right) with each subplot comparing experimental data with DL-based MCMC sampling.

sample sizes and provides a more accurate estimation of the underlying probability distribution. Fig. 22 compares the PDFs at different amplitude levels.

- At low amplitude, the match is good, but the MCMC samples show a slightly broader distribution compared to the experimental data
- At mid amplitude, there is a noticeable shift between the MCMC samples and experimental data, with the model predicting slightly higher frequencies.
- At high amplitude, the MCMC samples closely match the experimental data, with only a slight overestimation of the peak frequency.

The MCMC samples using the DL model generally capture the overall behaviour of the experimental system. There are small discrepancies in the predicted frequencies, especially at mid-amplitudes. The model form error can be a factor in this region, suggesting the approximated model may not fully capture some nonlinear effects that are more prominent in this range. The good match at low and high amplitudes indicates the model performs well at the extremes of the system's behaviour. This suggests that while the model is generally effective, there may be room for improvement in capturing certain nonlinear effects or sources of uncertainty in the system.

8. Conclusion

This study advances our understanding of uncertainty in nonlinear dynamic systems, particularly in joint structures, through stochastic modelling techniques. By integrating experimental data with analytical and deep learning (DL) models via Markov Chain Monte Carlo (MCMC) and Sparse Identification of Nonlinear Dynamics (SINDy), we provide a comprehensive analysis of system dynamics and uncertainties. Our approach leverages backbone curves for stochastic modelling, offering valuable insights into nonlinear behaviour.

The combination of SINDy, Phase-Locked Loop (PLL) methods, and DL significantly enhances modelling capabilities. SINDy provides a data-driven approach to identifying governing equations, PLL ensures accurate backbone curve extraction, and DL optimises computational efficiency. However, it is important to note that the use of an analytical model in Bayesian analysis, such as in MCMC, adds further to the computational cost due to the need for repeated model evaluations.

In this context, the DL model trained on both experimental data and data generated from the analytical model offers a compelling solution. It enables the replacement of computationally intensive numerical integration with a highly optimised inference process, reducing the overall computational burden without compromising accuracy. This hybrid approach allows for more efficient exploration of high-dimensional parameter spaces and accurate characterisation of uncertainties in jointed structures' behaviours.

However, challenges remain. The DL approach may face potential overfitting due to model complexity and limited training data. Future research will focus on applying this method to more complex systems, incorporating additional experimental data, and enhancing the DL architecture to improve generalisability and accuracy. This hybrid approach, combining data-driven modelling, physical insights from backbone curves, and DL's computational power, offers a comprehensive and efficient solution for stochastic modelling of complex dynamic systems. It enables better prediction of system responses under various conditions, aiding in improved design and maintenance decision-making.

CRediT authorship contribution statement

Pushpa Pandey: Writing – review & editing, Writing – original draft, Visualization, Validation, Software, Methodology, Investigation, Formal analysis, Data curation, Conceptualization. **Nidhal Jamia:** Writing – review & editing, Investigation, Formal analysis, Data curation. **Tanmoy Chatterjee:** Writing – review & editing, Supervision. **Hamed Haddad Khodaparast:** Writing – review & editing, Writing – original draft, Visualization, Supervision, Project administration, Methodology, Investigation, Funding acquisition, Data curation, Conceptualization. **Michael Ian Friswell:** Writing – review & editing, Writing – original draft, Visualization, Validation, Supervision, Project administration, Investigation, Funding acquisition, Data curation, Conceptualization.

Declaration of Generative AI and AI-assisted technologies in the writing process

The main text is written by the author and edited by coauthors. Claude, an AI language model developed by Anthropic, is used for proofreading in case of any grammatical errors.

Declaration of competing interest

The authors declare that they have no known competing financial interests or personal relationships that could have appeared to influence the work reported in this paper.

Funding and acknowledgement

The authors acknowledge the support of the Engineering and Physical Sciences Research Council, United Kingdom through the award of the Programme Grant “Digital Twins for Improved Dynamic Design”, grant number EP/R006768/1 and Tribomechadynamics Research Challenge for providing the experimental data. P. Pandey and Hamed Haddad Khodaparast acknowledge the funding from the RCUK Energy Programme [grant number EP/T012250/1].

Data availability

The datasets analysed during the current study are publicly available in the data repository [46]. The post-processing methods are provided via GitHub at https://github.com/maltekrack/NLtest.

References

[1] L. Gaul, J. Lenz, Nonlinear dynamics of structures assembled by bolted joints, Acta Mech. 125 (1–4) (1997) 169–181.
[2] M.I. Friswell, J.E. Mottershead, Finite Element Model Updating in Structural Dynamics, Springer Science & Business Media, 2010.
[3] H.H. Khodaparast, J.E. Mottershead, M.I. Friswell, Perturbation methods for the estimation of parameter variability in stochastic model updating, Mech. Syst. Signal Process. 22 (8) (2008) 1751–1773.
[4] F. Wang, V. Balakrishnan, Robust Kalman filters for linear time-varying systems with stochastic parametric uncertainties, IEEE Trans. Signal Process. 50 (4) (2002) 803–813.
[5] R. Mehra, On-line identification of linear dynamic systems with applications to Kalman filtering, IEEE Trans. Autom. Control 16 (1) (1971) 12–21.
[6] J.L. Beck, L.S. Katafygiotis, Updating models and their uncertainties. I: Bayesian statistical framework, J. Eng. Mech. 124 (4) (1998) 455–461.
[7] C. Mares, B. Dratz, J.E. Mottershead, M.I. Friswell, Model updating using Bayesian estimation, in: International Conference on Noise and Vibration Engineering, ISMA2006, Katholieke Universiteit Leuven, 2006, pp. 18–20.
[8] H.-P. Wan, W.-X. Ren, Stochastic model updating utilizing Bayesian approach and Gaussian process model, Mech. Syst. Signal Process. 70 (2016) 245–268.
[9] K. Xiong, H. Zhang, L. Liu, Adaptive robust extended Kalman filter for nonlinear stochastic systems, IET Control Theory Appl. 2 (3) (2008) 239–250.
[10] J.H. Lee, N.L. Ricker, Extended Kalman filter based nonlinear model predictive control, Ind. Eng. Chem. Res. 33 (6) (1994) 1530–1541.
[11] S.J. Julier, J.K. Uhlmann, New extension of the Kalman filter to nonlinear systems, in: Signal Processing, Sensor Fusion, and Target Recognition VI, vol. 3068, Spie, 1997, pp. 182–193.
[12] J. Carpenter, P. Clifford, P. Fearnhead, Improved particle filter for nonlinear problems, IEE Proc., Radar Sonar Navig. 146 (1) (1999) 2–7.
[13] B. Ristic, S. Arulampalam, N. Gordon, Beyond the Kalman Filter: Particle Filters for Tracking Applications, Artech house, 2003.
[14] S.H. Cheung, J.L. Beck, Bayesian model updating using hybrid Monte Carlo simulation with application to structural dynamic models with many uncertain parameters, J. Eng. Mech. 135 (4) (2009) 243–255.
[15] P.L. Green, K. Worden, Bayesian and Markov chain Monte Carlo methods for identifying nonlinear systems in the presence of uncertainty, Philos. Trans. R. Soc. A: Math. Phys. Eng. Sci. 373 (2051) (2015) 20140405.
[16] S. Bi, M. Beer, S. Cogan, J. Mottershead, Stochastic model updating with uncertainty quantification: an overview and tutorial, Mech. Syst. Signal Process. 204 (2023) 110784.
[17] P. Dutta, R. Bhattacharya, Nonlinear estimation with polynomial chaos and higher order moment updates, in: Proceedings of the 2010 American Control Conference, IEEE, 2010, pp. 3142–3147.
[18] R. Bhusal, K. Subbarao, Uncertainty quantification using generalized polynomial chaos expansion for nonlinear dynamical systems with mixed state and parameter uncertainties, J. Comput. Nonlinear Dyn. 14 (2) (2019) 021011.
[19] H. Moravej, T.H.T. Chan, K.D. Nguyen, A. Jesus, Vibration-based Bayesian model updating of civil engineering structures applying Gaussian process metamodel, Adv. Struct. Eng. 22 (16) (2019) 3487–3502.
[20] H. Jalali, H.H. Khodaparast, H. Madinei, M.I. Friswell, Stochastic modelling and updating of a joint contact interface, Mech. Syst. Signal Process. 129 (2019) 645–658.
[21] Y. Govers, H.H. Khodaparast, M. Link, J.E. Mottershead, A comparison of two stochastic model updating methods using the dlr AIRMOD test structure, Mech. Syst. Signal Process. 52 (2015) 105–114.

[22] E.P. Petrov, D.J. Ewins, Analytical Formulation of Friction Interface Elements for Analysis of Nonlinear Multi-Harmonic Vibrations of Bladed Disks , J. Turbomach. 125 (2) (2003) 364–371.
[23] G. Stefanou, The stochastic finite element method: Past, present and future, Comput. Methods Appl. Mech. Engrg. 198 (9) (2009) 1031–1051.
[24] M. Zhan, Q. Guo, L. Yue, B. Zhang, Modeling and stochastic model updating of bolt-jointed structure, Shock. Vib. 2018 (2018) 1–12.
[25] M. Peeters, R. Viguié, G. Sérandour, G. Kerschen, J.-C. Golinval, Nonlinear normal modes, part II: Toward a practical computation using numerical continuation techniques, Mech. Syst. Signal Process. 23 (1) (2009) 195–216.
[26] F. Müller, L. Woiwode, J. Gross, M. Scheel, M. Krack, Nonlinear damping quantification from phase-resonant tests under base excitation, Mech. Syst. Signal Process. 177 (2022) 109170.
[27] P. Hippold, M. Scheel, L. Renson, M. Krack, Robust and fast backbone tracking via phase-locked loops, Mech. Syst. Signal Process. 220 (2024) 111670.
[28] S.L. Brunton, J.L. Proctor, J.N. Kutz, Discovering governing equations from data by sparse identification of nonlinear dynamical systems, Proc. Natl. Acad. Sci. 113 (15) (2016) 3932–3937.
[29] S.H. Rudy, S.L. Brunton, J.L. Proctor, J.N. Kutz, Data-driven discovery of partial differential equations, Sci. Adv. 3 (4) (2017) 1602614.
[30] P. Pandey, H. H. Khodaparast, M. I. Friswell, T. Chatterjee, H. Madinei, T. Deighan, Stochastic nonlinear model updating in structural dynamics using a novel likelihood function within the Bayesian-MCMC framework, Appl. Math. Model. 138 (2025) 115800.
[31] M. Krack, M.R.W. Brake, C. Schwingshackl, J. Gross, P. Hippold, M. Lasen, D. Dini, L. Salles, M. Allen, D. Shetty, et al., The tribomechadynamics research challenge: Confronting blind predictions for the linear and nonlinear dynamics of a thin-walled jointed structure with measurement results, Mech. Syst. Signal Process. 224 (2025) 112016.
[32] A. Bhattu, S. Hermann, N. Jamia, F. Muller, M. Scheel, C.W. Schwingshackl, H.N. Özgüven, M. Krack, Experimental analysis of the TRC benchmark system, J. Struct. Dyn. [En Ligne], Spec. Issue Tribomechadynamics (2025).
[33] M. Scheel, S. Peter, R.I. Leine, M. Krack, A phase resonance approach for modal testing of structures with nonlinear dissipation, J. Sound Vib. 435 (2018) 56–73.
[34] G. Kerschen, M. Peeters, J.C. Golinval, A.F. Vakakis, Nonlinear normal modes, part I: A useful framework for the structural dynamicist, Mech. Syst. Signal Process. 23 (1) (2009) 170–194.
[35] J. Taghipour, H.H. Khodaparast, M.I. Friswell, A.D. Shaw, H. Jalali, N. Jamia, Harmonic-balance-based parameter estimation of nonlinear structures in the presence of multi-harmonic response and force, Mech. Syst. Signal Process. 162 (2022) 108057.
[36] C. Mares, J.E. Mottershead, M.I. Friswell, Stochastic model updating: Part 1—theory and simulated example, Mech. Syst. Signal Process. 20 (7) (2006) 1674–1695.
[37] J. Daunizeau, K.J. Friston, S.J. Kiebel, Variational Bayesian identification and prediction of stochastic nonlinear dynamic causal models, Phys. D: Nonlinear Phenom. 238 (21) (2009) 2089–2118.
[38] C. Papadimitriou, Bayesian uncertainty quantification and propagation (UQ+P): State-of-the-art tools for linear and nonlinear structural dynamics models, in: E. Chatzi, C. Papadimitriou (Eds.), Identification Methods for Structural Health Monitoring, Springer International Publishing, 2016, pp. 137–170.
[39] Y. Huang, C. Shao, B. Wu, J.L. Beck, H. Li, State-of-the-art review on Bayesian inference in structural system identification and damage assessment, Adv. Struct. Eng. 22 (6) (2019) 1329–1351.
[40] Z. Taherkhani, H. Ahmadian, Stochastic model updating of rotor support parameters using Bayesian approach, Mech. Syst. Signal Process. 158 (2021) 107702.
[41] W.K. Hastings, Monte Carlo sampling methods using Markov chains and their applications, Biometrika 57 (1) (1970) 97–109.
[42] P.J. Li, D.W. Xu, J. Zhang, Probability-based structural health monitoring through Markov chain Monte Carlo sampling, Int. J. Struct. Stab. Dyn. 16 (07) (2016) 1550039.
[43] S. Wu, P. Angelikopoulos, C. Papadimitriou, P. Koumoutsakos, Bayesian annealed sequential importance sampling: an unbiased version of transitional Markov chain Monte Carlo, ASCE- ASME J. Risk Uncertain. Eng. Syst. Part B: Mech. Eng. 4 (1) (2018) 011008.
[44] F. Schneider, I. Papaioannou, D. Straub, C. Winter, G. Müller, Bayesian parameter updating in linear structural dynamics with frequency transformed data using rational surrogate models, Mech. Syst. Signal Process. 166 (2022) 108407.
[45] Francisco de Castro, Fitmethis, 2025, MATLAB Central File Exchange.
[46] A. Bhattu, S. Hermann, N. Jamia, F. Muller, M. Scheel, C.W. Schwingshackl, H.N. Özgüven, M. Krack, TRChallenge - experimental results 2022, 2024.